arXiv:cond-mat/9901246v2 [cond-mat.mtrl-sci] 12 Mar 1999

# Lattice dynamics of $BaTiO_3$, $PbTiO_3$ and $PbZrO_3$: a comparative first-principles study

Ph. Ghosez, E. Cockayne*, U. V. Waghmare** and K. M. Rabe
*Department of Applied Physics, Yale University, P.O. Box 208284, New Haven, CT 06520-8284, USA.*

(February 1, 2008)

The full phonon dispersion relations of lead titanate and lead zirconate in the cubic perovskite structure are computed using first-principles variational density-functional perturbation theory, with ab initio pseudopotentials and a plane-wave basis set. Comparison with the results previously obtained for barium titanate shows that the change of a single constituent (Ba to Pb, Ti to Zr) has profound effects on the character and dispersion of unstable modes, with significant implications for the nature of the phase transitions and the dielectric and piezoelectric responses of the compounds. Examination of the interatomic force constants in real space, obtained by a transformation which correctly treats the long-range dipolar contribution, shows that most are strikingly similar, while it is the differences in a few key interactions which produce the observed changes in the phonon dispersions. These trends suggest the possibility of the transferability of force constants to predict the lattice dynamics of perovskite solid solutions.

## I. INTRODUCTION

In the family of perovskite $ABO_3$ compounds, a wide variety of distorted variants of the high-temperature cubic structure are observed as a function of composition and temperature [1]. First-principles density-functional energy-minimization methods have proved to be generally quite accurate in the theoretical prediction of the ground state structure type and structural parameters of perovskite oxides [2]. According to the soft-mode theory of structural phase transitions, the ferroelectric phases can be related to the high temperature symmetric structure by the freezing-in of unstable zone-center phonons. However, to predict finite temperature behavior at phase transitions, as well as the temperature dependence of the dielectric and piezoelectric responses of the compounds, it is necessary to have information about the energies of *non-uniform* instabilities and low energy distortions of the cubic perovskite structure [3]. For this purpose, the calculation of the phonon dispersion relations through density-functional perturbation theory (DFPT) [4,5] has been found to be extremely useful, allowing easy identification of the unstable phonon branches and their dispersion throughout the Brillouin zone. This information also permits the investigation of the geometry of localized instabilities in real space, which can be directly related to the anisotropy of the instability region in reciprocal space [6,7,8]. To date, phonon calculations away from the zone center have been reported for only a few individual compounds, with full phonon dispersion relations given for $KNbO_3$ [6], $SrTiO_3$ [9] and $BaTiO_3$ [8], and selected eigenmodes for $PbTiO_3$ [10].

In this paper, we present the first comparative study of the full phonon dispersion relations of three different cubic perovskites: $BaTiO_3$, $PbTiO_3$ and $PbZrO_3$, computed from first principles using the variational DFPT method as described in Section II. These compounds have been chosen both because of their scientific and technological importance, and because they allow us to investigate the effects on the lattice dynamics of substituting one cation with the other atoms unchanged. As we will see in Sections III and IV, these substitutions lead to very pronounced differences in the eigenvectors and dispersions of the unstable phonons. The origin of these differences will be clarified in Section V, where, using a systematic method previously applied to $BaTiO_3$ [8], the reciprocal space force constant matrices are transformed to obtain real-space interatomic force constants for all three compounds. There, we will see that the differences can be attributed to trends in cation-oxygen interactions, with other IFCs remarkably similar among the three compounds. These trends and similarities, and their implications for the study of the lattice dynamics of solid solutions, are discussed in Section V. Section VI concludes the paper.

## II. METHOD

The first-principles calculations for $BaTiO_3$ follow the method previously reported in Ref. [8]. For $PbTiO_3$ and $PbZrO_3$, calculations were performed within the Kohn-Sham formulation of density functional theory [11], using the conjugate-gradients method [12]. The exchange-correlation energy functional was evaluated within the local density approximation (LDA), using the Perdew-Zunger parametrization [13] of the Ceperley-Alder [14] homogeneous electron gas data [15]. The "all-electron" potentials were replaced by the same *ab initio* pseudopotentials as in Refs. [10] and [16]. The electronic wavefunctions were expanded in plane waves up to a kinetic energy cutoff of 850 eV. Integrals over the Brillouin zone were approximated by sums on a $4\times4\times4$ mesh of special $k$-points [17].

The optical dielectric constant, the Born effective charges and the force constant matrix at selected $q$-points of the Brillouin zone were computed within a variational formulation [5] of density functional perturbation theory [4]. The phonon dispersion curves were interpolated following the scheme described in Ref. [18,19]. In this approach, the long-range character of the dipole-dipole contribution is correctly handled by first subtracting it from the force constant matrix in reciprocal space and treating it separately. The short-range contribution to the interatomic force constants in real space is then obtained from the remainder of the force constant matrix in $q$-space using a discrete Fourier transformation. In this work, the short-range contribution was computed from the force constant matrices on a $2 \times 2 \times 2$ centered cubic mesh of $q$-points comprised of $\Gamma$, X, M, R and the $\Lambda$ point halfway from $\Gamma$ to R [20]. From the resulting set of interatomic force constants in real space, the phonon spectrum can be readily obtained at any point in the Brillouin zone.

Our calculations have been performed in the cubic perovskite structure. For $PbTiO_3$, the optimized LDA lattice parameter (3.883 Å) slightly underestimates the experimental estimated value of 3.969 Å [21] and we have decided to work, as for $BaTiO_3$ [8], at the experimental volume. For $PbZrO_3$, we have chosen, as in Ref. [22], to work at the optimized lattice parameter of 4.12 Å, which is nearly indistinguishable from the extrapolated experimental value of 4.13 Å [23].

## III. DIELECTRIC PROPERTIES

Knowledge of the Born effective charges ($Z^*_\kappa$) and the optical dielectric tensor ($\epsilon_\infty$) is essential for describing the long-range dipolar contribution to the lattice dynamics of a polar insulator. In Table I, we present results for $PbTiO_3$ and $PbZrO_3$, computed using the method described in Section II, and for $BaTiO_3$, obtained previously in Ref. [8]. The effective charges have been corrected following the scheme proposed in Ref. [24] in order to satisfy the charge neutrality sum rule. Our results differ by at most 0.09 electrons with values reported for cubic $PbTiO_3$ and $PbZrO_3$ using slightly different methods and/or lattice constants [10,16,25].

As usual in the class of perovskite $ABO_3$ compounds, the amplitudes of some elements of the effective charge tensors deviate substantially from the nominal value expected in a purely ionic picture (for a review, see for instance Ref. [26]). This effect is especially pronounced for the Ti and associated $O_\parallel$ charges in $BaTiO_3$ and $PbTiO_3$. It reflects the sensitivity to atomic displacement of the partially-covalent character of the Ti–O bond [27]. In contrast, the effective charge of the Zr atom in $PbZrO_3$ and the associated $O_\parallel$ charge are significantly closer to their nominal ionic values of +4 and −2, respectively. The Zr effective charge is comparable to that reported recently for $ZrO_2$ (+5.75) [28]. In addition, in both $PbTiO_3$ and $PbZrO_3$, the *anomalous* contribution to the Pb charge, beyond the nominal charge of +2, is more than twice as large as that for the Ba charge in $BaTiO_3$. This feature, too, with a concomitent increase in the magnitude of $Z^*_{O\perp}$, reflects the sensitivity to atomic displacement of the partially covalent character of the bond between lead and oxygen.

Within the LDA, the computed optical dielectric constant (Table I) usually overestimates the experimental value. The error is of the order of 20% in $BaTiO_3$ [30], for which the extrapolated experimental value is 5.40 [31], consistent with analogous comparisons in $KNbO_3$ [32] and $SrTiO_3$ [9]. For $PbZrO_3$, it appears that experimental data is available only for the orthorhombic phase, where the value is about 4.8 [33], significantly less than the value of 6.97 which we have computed for the cubic phase. For $PbTiO_3$, our value of 8.24 is comparable to a recent first-principles result of 8.28 obtained using a different method [34]. In contrast to the other perovskites, this represents a slight underestimate of the extrapolated experimental value of 8.64 reported in Ref. [25].

The origin of the LDA error in the optical dielectric constant is a complex question. It arises at least partly from the lack of polarization dependence of the approximate exchange-correlation functional [29]. In the cubic phase of the perovskite ferroelectrics, the comparison with experiment is also complicated by the fact that the high-temperature cubic phases for which the measurements are made do not have a perfect cubic perovskite structure, as assumed in the calculations. In fact, the observed cubic structure of $BaTiO_3$ and $PbTiO_3$ represents the average of large local distortions. The character of these distortions depends strongly on the material, which could well have different effects on the observed optical dielectric constant.

For the $BaTiO_3$ phonon dispersion, it has been checked that the inaccuracy in $\epsilon_\infty$ only significantly affects the position of the highest longitudinal optic branch, while other frequencies are relatively insensitive to the amplitude of the dielectric constant [8]. The effects of possible discrepancies for the other two compounds are likely to be similarly minor.

## IV. PHONON DISPERSION CURVES

In this section, we describe phonon dispersion relations for $BaTiO_3$, $PbTiO_3$ and $PbZrO_3$, providing a global view of the quadratic-order energy surface around the cubic perovskite structure. The calculated phonon dispersion curves along the high symmetry lines of the simple cubic Brillouin zone are shown in Fig. 1. The unstable modes, which determine the nature of the phase transitions and the dielectric and piezoelectric responses of the compounds, have imaginary frequencies. Their dispersion is shown below the zero-frequency line. The character of these modes also has significant implications for the properties of the system. This character has been depicted in Fig. 1 by assigning a color to each eigenvalue, determined by the percentage of each atomic character in the normalized eigenvector of the dynamical matrix (red for A atom, green for B atom and blue for O atoms) [35].

Barium titanate ($BaTiO_3$) and potassium niobate ($KNbO_3$) both undergo a transition sequence with decreasing temperature through ferroelectric tetragonal, orthorhombic and rhombohedral (ground state) structures, all related to the cubic perovskite structure by the freezing-in of a polar mode at $\Gamma$. The main features of the phonon dispersion of $BaTiO_3$ have been previously discussed in Ref. [8] and are very similar to those of $KNbO_3$ [6]. The most unstable mode is at $\Gamma$, and this mode, dominated by the Ti displacement against the oxygens (Table II), is the one that freezes in to give the ferroelectric phases. However, the instability is not restricted to the $\Gamma$ point. Branches of Ti-dominated unstable modes extend over much of the Brillouin zone. The flat dispersions of the unstable transverse optic mode towards X and M, combined with its rapid stiffening towards R, confine the instability to three quasi-two-dimensional "slabs" of reciprocal space intersecting at $\Gamma$. This is the fingerprint of a "chain-like" unstable localized distortion for the Ti displacements in real space [6,8]. Except for these modes, all the other phonons are stable in $BaTiO_3$, which makes the behavior of the unstable branches relatively easy to understand.

Lead titanate ($PbTiO_3$) has a single transition to a low-temperature ferroelectric tetragonal structure, related to the cubic perovskite structure by the freezing-in of a polar mode at $\Gamma$. The phonon dispersion of $PbTiO_3$ shows similar features to that of $BaTiO_3$, with some important differences. As in $BaTiO_3$, the most unstable mode is at $\Gamma$, consistent with the observed ground state structure. However, the eigenvector is no longer strongly dominated by the displacement of the Ti against the oxygen along the Ti–O chains, but contains a significant component of the Pb moving against the O atoms in the Pb–O planes (see Table II). Unstable Ti-dominated modes, similar to those in $BaTiO_3$, can be identified in the vicinity of the M–X line ($M_{3'}$, $X_5$ modes). However, Pb now plays an active role in the character of the majority of the unstable branches, notably those terminating at $M_{5'}$ and $X_{5'}$. Also, the Pb-dominated branch emanating from the ferroelectric $\Gamma$ mode towards R has a much weaker dispersion than the corresponding, Ti-dominated, branch in $BaTiO_3$. In consequence, the unstable localized ferroelectric distortion in real space is nearly isotropic, in contrast to the pronounced anisotropy in $BaTiO_3$. Finally, there is an antiferrodistortive instability at the R-point ($R_{25}$ mode). As similarly observed in $SrTiO_3$ [9], this instability is confined to quasi-one-dimensional "tubes" of reciprocal space running along the edges of the simple cubic Brillouin zone ($R_{25}$ and $M_3$ modes and the branch connecting them). The branches emanating from this region stabilize rapidly away from the Brillouin zone edge towards, in particular, $\Gamma_{25}$ and $X_3$. In real space, this instability appears as a cooperative rotation of oxygen octahedra, with strong correlations in the plane perperpendicular to the axis of rotation, and little correlation between rotations in different planes. The lack of interplane correlation, arising from the flatness of the $R_{25}$–$M_3$ branch, suggests the absence of coupling between the oxygen motion in different planes. This will be discussed further in the next section.

The ground state of $PbZrO_3$ is an antiferroelectric with 8 formula units per unit cell, obtained by freezing in a set of coupled modes, most importantly modes at R and $\Sigma(\frac{1}{4}\frac{1}{4}0)$ [36]. The phonon dispersion correspondingly shows even more pronounced and complex instabilities than for $PbTiO_3$. Overall, the unstable branches are dominated by Pb and O displacements, with no significant Zr character. There is still a polar instability at the $\Gamma$ point but the eigenvector (see Table II) is clearly dominated by the displacement of lead against the oxygens while the Zr atom now moves *with* these oxygens. In fact, the modes where the Zr is displaced against the oxygens ($\Gamma_{LO}$ at 160 $cm^{-1}$, $M_{3'}$, $X_5$ modes) are now all stable. The octahedral rotation branch is again remarkably flat and is significantly more unstable at $R_{25}$ and $M_3$ than in $PbTiO_3$. The antiferrodistortive instability retains some one-dimensional character but spreads into a larger region of reciprocal space : the $\Gamma_{25}$ and $X_3$ transverse oxygen motions, related to the $R_{25}$ mode, are still stable but with a relatively low frequency. We note finally that the stiffest longitudinal and tranverse oxygen branches have been shifted to higher energy relative to the titanates.

## V. INTERATOMIC FORCE CONSTANTS

In the previous section, comparisons between the three compounds were made by analyzing phonon dispersion relations along high-symmetry lines in reciprocal space. A complementary, highly instructive picture of the quadratic-order structural energetics of the system is provided by direct examination of the real-space interatomic force constants (IFC).

The interatomic force constants (IFC) are generated in the construction of the phonon dispersion relations; their computation has been described in Section II. Our convention is that the IFC matrix $C_{\alpha,\beta}(l\kappa, l'\kappa')$ which relates the force $F_\alpha(l\kappa)$ on atom $\kappa$ in cell $l$ and the displacement $\Delta\tau_\beta(l'\kappa')$ of atom $\kappa'$ in cell $l'$ is defined through the following expression: $F_\alpha(l\kappa) = -C_{\alpha,\beta}(l\kappa, l'\kappa').\Delta\tau_\beta(l'\kappa')$. Moreover, the total IFC can be decomposed into a dipole-dipole part (DD) and a short-range part (SR) , following Refs. [19,37]. Such a decomposition is somewhat arbitrary but is useful for understanding the microscopic origin of the trends among different compounds. For convenience, the atoms are labeled according to Table III, as illustrated in Fig. 2. The interatomic force constants are reported either in cartesian coordinates or in terms of their longitudinal (‖) and transverse (⊥) contributions along the line connecting the two atoms. The results for $BaTiO_3$, $PbTiO_3$ and $PbZrO_3$ are presented in Tables IV, V and VI.

First, we examine the "self-force constant," which specifies the force on a single isolated atom at a unit displacement from its crystalline position, all the other atoms remaining fixed. The values are given in Table IV. The self-force constants are positive for all atoms in the three compounds, so that all three are stable against isolated atomic displacements. Therefore, it is only the cooperative motion of different atoms that can decrease the energy of the crystal and generate an instability, such as is observed in the phonon dispersion relations presented in the previous Section. The analysis of the IFCs will help us to identify the energetically favorable coupling in the displacements and elucidate the origin of the unstable phonon branches.

Next, we discuss the ferroelectric instability at Γ, and the phonon branches which emanate from it. In barium titanate, it was found that the unstable eigenvector is dominated by Ti displacement along the Ti–O–Ti chain. If we consider the simple case where only Ti atoms are allowed to displace, we find that the destabilizing contribution from the $Ti_0$–$Ti_1$ ‖ interaction itself is nearly enough to compensate the Ti self-force constant (Table V). In addition, the fact that the $Ti_0$–$Ti_1$ ⊥ interaction is comparatively small can account directly for the characteristic flat dispersion along Γ-X and Γ-M and the strong stiffening along Γ-R, associated with the chain-like nature of the instability. For the true eigenvector, another important, though relatively small, destabilizing contribution comes from the cooperative displacement of the $O_1$ atoms against the titaniums along the Ti–O chains. This, together with the total contribution of the rest of the IFCs, is responsible for the actual instability of the ferroelectric Ti-dominated branches in $BaTiO_3$.

For lead titanate, the energetics of the Ti-only displacements, dominated by the Ti self-force constant and the $Ti_0$–$Ti_1$ ‖ and ⊥ interactions, are remarkably similar to those in $BaTiO_3$ (Table V). However, in $PbTiO_3$ there is also an important destabilization associated with pure Pb displacements [38]. This can be fully attributed to the large difference in the Ba and Pb self-force constants, while the $A_0$–$A_1$ ‖ and ⊥ interactions are very similar in the two compounds. Also, the $A_0$–$B_0$ ‖ and ⊥ cation interactions are of the same order of magnitude as in $BaTiO_3$ and combine to give a surprisingly small $xx$ coupling. At Γ, symmetry considerations permit the mixing of Ti–O and Pb–O displacements and in the phonon branches which emanate from it, thus accounting for the nature of the ferroelectric eigenvector. However, at X, M and R symmetry labels distinguish the Ti-dominated ($X_5$, $M_{3'}$ and $R_{25'}$) and Pb-dominated ($X_{5'}$, $M_{2'}$ and $R_{15}$) modes, which can be readily identified in the calculated phonon dispersion. Also, the $Pb_0$–$Pb_1$ coupling is much smaller in magnitude than the $Ti_0$–$Ti_1$ coupling, which accounts for the relatively weak dispersion of the Pb-dominated branch from Γ to R. In the true eigenvectors, these instabilities are further reinforced by displacements of the oxygens. While the longitudinal IFC between $Ba_0$ and $O_1$ was very small in $BaTiO_3$, there is a significant destabilizing interaction between $Pb_0$ and $O_1$ in $PbTiO_3$, which further promotes the involvement of Pb in the unstable phonon branches. We note that the $Ti_0$–$O_1$ longitudinal interaction is repulsive in $PbTiO_3$, but it is even smaller in amplitude than in $BaTiO_3$ and its stabilizing effect is compensated by the transverse coupling between Pb and $O_1$.

In lead zirconate, the unstable eigenvector at Γ is strongly dominated by Pb–O motion, with little involvement of Zr. This can be understood by comparing, in Table V, the energetics of Zr-only displacements with those of Ti-only displacements in $PbTiO_3$ and $BaTiO_3$: the Zr self-force constant is significantly larger and the $Zr_0$–$Zr_1$ ‖ and ⊥ interactions are smaller, so that Zr cannot move as easily as Ti. Also, the $Zr_0$–$O_1$ ‖ interaction is now significantly repulsive, explaining why the Zr atom does not move against the oxygens, but with them. As for the titanates, we note finally that the Zr atoms are mainly coupled along the B–O chains, so that the characteristic dispersion of the B-atom modes is preserved, only at higher frequencies. On the other hand, the Pb self-force constant is much smaller, the $Pb_0$–$Pb_1$ ‖ and ⊥ interactions are only slightly smaller, and the destabilizing coupling between lead and oxygen is similar to that in $PbTiO_3$, accounting for the involvement of Pb in the instability.

Finally, we discuss the antiferrodistortive instability identified with the $R_{25}$ and $M_3$ modes and the branch along R–M connecting them. There is a marked variation in the frequency of the $R_{25}$ mode in the three compounds, ranging from the lack of any instability in $BaTiO_3$, to $PbTiO_3$ with an unstable $R_{25}$ mode that nonetheless does not contribute to the ground state, and finally to $PbZrO_3$ in which the $R_{25}$ mode is even more unstable and contributes significantly to the observed ground state [36]. The eigenvector of this mode is completely determined by symmetry and corresponds to a coupled rotation of the corner-connected oxygen octahedra. Its frequency depends only on the oxygen IFCs, predominantly the self-force constant and the off-diagonal coupling between nearest neighbor oxygen atoms. In fact, the latter (for example, $O_{1y}$–$O_{2z}$ in Table VI) is remarkably similar in all three compounds. The trend is therefore associated with the rapid decrease in the transverse O self-force constant from $BaTiO_3$ to $PbTiO_3$ to $PbZrO_3$ and the resulting compensation of the contribution from the self-force constant by the destabilizing contribution from the off-diagonal coupling.

The self-force constant can be written as a sum over interatomic force constants, according to the requirement of translational invariance: $C_{\alpha,\beta}(l\kappa,l\kappa) = -\sum'_{l'\kappa'} C_{\alpha,\beta}(l\kappa,l'\kappa')$. It is therefore of interest to identify which interatomic force constants are responsible for the trend in the transverse oxygen self-force constant. The suggestion that the trend is due to covalency-induced changes in the Pb–O interactions can be directly investigated through a "computer experiment." Everything else being equal, we artificially replace the IFC between $A_0$ and $O_1$ atoms in $BaTiO_3$ by its value in $PbTiO_3$, consequently modifying the self-force constant on A and O atoms. For this hypothetical material, the A-atom dominated modes are shifted to lower frequencies while the frequency of the $R_{25}$ mode is lowered to $40i$ cm$^{-1}$. If we introduce the stronger $A_0$–$O_1$ interaction of $PbZrO_3$, we obtain an even larger $R_{25}$ instability of $103i$ cm$^{-1}$.

The previous simulation demonstrates the crucial role played by the lead-oxygen interaction in generating the AFD instability. However, this change alone is not sufficient to reproduce the flatness of the $R_{25}$–$M_3$ branch, as the corresponding frequencies of the $M_3$ mode in the two hypothetical cases above are 92 cm$^{-1}$ and $25i$ cm$^{-1}$, respectively. Naively, the absence of dispersion of the antiferrodistortive mode along that line would be interpreted as the absence of coupling between the oxygens in the different planes. However, as can be seen in Table VI, the $yy$ transverse coupling between $O_1$ and $O_3$ is far from negligible, and acts to amplify the AFD instability at R with respect to M. In the lead compounds, however, this is compensated by another $yz$ coupling, between $O_1$ and $O_5$. The latter is significantly smaller in $BaTiO_3$ (by 35 %). If we consider a third hypothetical compound in which this coupling in $BaTiO_3$ is additionally changed to its value in $PbTiO_3$, we recover a flat behavior along the R–M line. In the lead perovskites, the flatness of this band appears therefore as a consequence of a compensation between different interplane interactions, and cannot be attributed to complete independence of oxygen motions in the different planes.

## VI. DISCUSSION

In Section IV, we observed marked differences between the phonon dispersion relations and eigenvectors in the three related compounds. Through the real-space analysis in the previous section, we have seen that these differences arise from changes in a few key interatomic force constants.

First, we remark that B–O interactions depend strongly on the B atom, being similar in $PbTiO_3$ and $BaTiO_3$, and quite different in $PbZrO_3$. In fact, the SR force contribution to the $Zr_0$–$O_1$ interaction and $Ti_0$–$O_1$ are very similar, so that the difference arises from the dipolar contribution. In $PbZrO_3$, this contribution is reduced in consequence of the lower values of the Born effective charges (see Table V). This trend provides another example of the *very* delicate nature of the compensation between SR and DD forces, previously pointed out for $BaTiO_3$ [39,37].

Next, we remark that A–O interactions depend strongly on the A atom, being similar in $PbTiO_3$ and $PbZrO_3$, and quite different in $BaTiO_3$. This change originates in the covalent character of the bonding between Pb and O, which results both in smaller A–O SR coupling and a larger Born effective charge for Pb. Even though the impact of the latter on destabilizing the DD interaction is partly compensated by the increased $\epsilon_\infty$, the net effect is to promote the Pb–O instability.

As discussed above, the self-force constant can be written as a sum over interatomic force constants. It can be easily verified that the trends in the self-force constants observed in Table III are primarily associated with the trends in A–O and B–O interactions.

The rest of the IFCs given in Table VI are actually remarkably similar. For example, A–B interactions are apparently insensitive to the identity of A (Ba, Pb) or B (Ti, Zr). This is true also for A–A, B–B and most O–O interactions. The small differences observed can at least in part be attributed to differences in the lattice constants and in $\epsilon_\infty$ for the three compounds.

The similarities in IFC's among compounds with related compositions offer an intriguing opportunity for the modelling of the lattice dynamics of solid solutions. In the simplest case, the lattice dynamics of ordered supercells of compounds such as PZT could be obtained by using the appropriate A–O and B–O couplings from the pure compounds and averaged values for the A–B, A–A, B–B and O–O interactions. In a more sophisticated treatment, the dipolar contributions could be separately handled within an approach correctly treating the local fields and Born effective charges. Implementation of these ideas is in progress.

## VII. CONCLUSIONS

In this paper, we have described in detail the first-principles phonon dispersion relations and real-space interatomic force constants of cubic $PbTiO_3$ and $PbZrO_3$ and compared them with results previously obtained for $BaTiO_3$. The modifications induced by the substitution of Ba by Pb and of Ti by Zr are seen to be most easily understood by considering the real-space IFCs. The replacement of Ba by Pb strongly strengthens the A–O coupling, which is directly responsible for both the involvement of Pb in the ferroelectric eigenvector and the appearance of the antiferrodistortive instability. The two-dimensional real-space character of the latter results from an additional slight modification of the O–O coupling. The replacement of Ti in $PbTiO_3$ by Zr strongly modifies the B–O interaction, suppressing the involvement of Zr in the unstable modes of $PbZrO_3$. The decrease of the Born effective charges along the B–O bonds is a crucial factor in modifying this interaction. In addition, the substitution of Ti by Zr slightly strengthens the Pb–O coupling. Apart from these modifications, the other IFCs are remarkably similar in the three compounds studied. The consequent prospects for transferability to solid solutions were discussed.

## ACKNOWLEDGMENTS

The authors thank Ch. LaSota and H. Krakauer for communicating unpublished results concerning $SrTiO_3$ as well as X. Gonze for the availability of the ABINIT package, helpful for the interpolation of the phonon dispersion curves and the analysis of the interatomic force constants. PhG, UVW and KMR acknowledge useful discussions with many participants in the 1998 summer workshop “The Physics of Insulators” at the Aspen Center for Physics, where part of this work was performed. This work was supported by ONR Grant N00014-97-0047. EC received partial funding from an NRC Postdoctoral Fellowship and from Sandia National Laboratories. Sandia is a multi-program national laboratory operated by the Sandia Corporation, a Lockheed Martin Company, for the United States Department of Energy under contract DE-AL04-94AL8500.

---

[*] Present address: National Institute of Standards and Technology, Ceramics Division, Gaithersburg, MD 20899-8520.

[**] Present address: Department of Physics, Harvard University, Cambridge, MA 02138.

[1] M. E. Lines and A. M. Glass, *Principles and Applications of Ferroelectrics and Related Materials* (Clarendon Press, Oxford, 1977).

[2] D. Vanderbilt, Current Opinions in Solid State and Materials Science **2**, 701 (1997).

[3] K. M. Rabe and U. V. Waghmare, Ferroelectrics **136**, 147 (1992); *ibid.* **164**, 15 (1995).

[4] N. E. Zein, Sov. Phys. Solid State **26**, 1825 (1984); S. Baroni, P. Giannozzi and A. Testa, Phys. Rev. Lett. **58**, 1861 (1987).

[5] X. Gonze, D.C. Allan, and M.P. Teter, Phys. Rev. Lett. **68**, 3603 (1992).

[6] R. Yu and H. Krakauer, Phys. Rev. Lett. **74**, 4067 (1995).

[7] K. M. Rabe and E. Cockayne, in *First-principles Calculations for Ferroelectrics*, edited by R.E. Cohen, AIP Conf. Proc. No. 436 (AIP, Woodbury, 1998), p. 139.

[8] Ph. Ghosez, X. Gonze, and J.-P. Michenaud, Ferroelectrics **206**, 205 (1998).

[9] C. LaSota, C-Z. Wang, R. Yu, and H. Krakauer, Ferroelectrics **194**, 109 (1997); C. Lasota and H. Krakauer, private communication.

[10] U.V. Waghmare and K.M. Rabe, Phys.Rev. B **55**, 6161 (1997).

[11] P. Hohenberg and W. Kohn, Phys. Rev. **136**, B864 (1964); W. Kohn and L.-J. Sham, Phys. Rev. **140**, A1133 (1965).

[12] M. C. Payne, M.P. Teter, D.C. Allan, T.A. Arias and J.D. Joannopoulos, Rev. Mod. Phys. **64**, 1045 (1992).

[13] J. P. Perdew and A. Zunger, Phys. Rev. B **23**, 5048 (1981).

[14] D. M. Ceperley and B.J. Alder, Phys. Rev. Lett. **45**, 566 (1980).

[15] In our version of the CASTEP code, the XC energy density ($\epsilon_{xc}$) and XC potential ($v_{xc}$) are first evaluated on a grid from the Perdew-Zunger analytical expression. During the computation, the values of $\epsilon_{xc}$ and $v_{xc}$ at a given $r_s$ are then interpolated using to a third-order polynomial fit of the grid values in the region of interest (i.e. using the 4 grid points closest to the given $r_s$). In our DFPT calculation, the exchange part of the XC kernel ($K_{xc}$) has been treated exactly while the correlation contribution was evaluated from the first derivative of a third-order polynomial fit of the grid values of the XC potential. This technique, by smoothing out the $v_{xc}$ curve, eliminates the problem associated with the discontinuity at $r_s = 1$ of the second derivative of Perdew-Zunger exchange-correlation energy analytical expression. The resulting difference between force constants determined from frozen phonon and DFPT calculations is negligible. For example, using this technique in $PbTiO_3$ gives the diagonal matrix element at $\Gamma$ associated with the displacement of oxygen in the Pb–O plane as 3.3337 eV/Å$^2$, while the frozen phonon value is equal to 3.3328 eV/Å$^2$. Further details will be described in a separate publication.

[16] U.V. Waghmare and K.M. Rabe, Ferroelectrics **194**, 135 (1997).

[17] H. J. Monkhorst and J. D. Pack, Phys. Rev. B **13**, 5188 (1976); ibid., Phys. Rev. B **16**, 1748 (1977).

[18] P. Giannozzi, S. de Gironcoli, P. Pavone, and S. Baroni, Phys. Rev. B **43**, 7231 (1991).

[19] X. Gonze, J.-C. Charlier, D.C. Allan, and M.P. Teter, Phys. Rev. B **50**, 13035 (1994).

[20] Discrete Fourier transform from a $2 \times 2 \times 2$ simple cubic (SC) mesh of $q$-points would limit the range of the SR part of the IFC to a $2 \times 2 \times 2$ supercell in real space. Our BCC mesh summarizes the information of two SC meshes shifted with respect to each other by a vector $q$ =(0.25, 0.25, 0.25).

[21] T. Mitsui et al., *Landolt-Bornstein Numerical Data and Functional Relationships in Science and Technology* (Springer-Verlag, 1981), NS, III/16.

[22] D. J. Singh, Phys. Rev. B **52**, 12559 (1995).

[23] E. Sawaguchi, J. Phys. Soc. Japan **8**, 615 (1953).

[24] X. Gonze and Ch. Lee, Phys. Rev. B **55**, 10355 (1997).

[25] W. Zhong, D. King-Smith and D. Vanderbilt, Phys. Rev. Lett. **72**, 3618 (1994).

[26] Ph. Ghosez, J.-P. Michenaud, and X. Gonze, Phys. Rev. B **58**, 6224 (1998).

[27] W. A. Harrison, *Electronic Structure and the Properties of Solids: the Physics of the Chemical Bond* (W. H. Freeman and Co., San Francisco, 1980).

[28] F. Detraux, Ph. Ghosez and X. Gonze, Phys. Rev. Lett. **81**, 3297 (1998).

[29] X. Gonze, Ph. Ghosez and R. W. Godby, Phys. Rev. Lett. **74**, 4035 (1995).

[30] Ph. Ghosez, X. Gonze, and J.-P. Michenaud, Ferroelectrics **164**, 113 (1995).

[31] $\epsilon_\infty$ was obtained by extrapolating refractive index measurements at different wavelengths [G. Burns and F. H. Dacol, Solid State Comm. 42, 9 (1982)] to zero frequency, using a one oscillator Sellmeyer equation.

[32] C.-Z. Wang, R. Yu, and H. Krakauer, Phys. Rev. B **54**, 11161 (1996).

[33] F. Jona, G. Shirane and P. Pepinsky, Phys. Rev **6**, 1584 (1955).

[34] F. Bernardini and V. Fiorentini, Phys. Rev. B **58**, 15292 (1998).

[35] For example, a normalized mode with A displacement 0.7, B displacement 0.5, and O displacements 0.5, 0.1, and 0.0 (in generalized coordinates) would be colored via the command “0.49 0.25 0.26 setrgbcolor” in the Adobe Systems Inc. PostScript$^{TM}$ language.

[36] H. Fujishita and S. Hoshino, J. Phys. Soc. Japan **53**, 226 (1984).

[37] Ph. Ghosez, X. Gonze and J.-P. Michenaud, Ferroelectrics **194**, 39 (1997).

[38] Specifically, the Pb diagonal element of the full force constant matrix at Γ ($-0.0018$ Ha/Bohr$^2$) shows that uniform Pb displacement is unstable. This is not the case for Ba in $BaTiO_3$.

[39] Ph. Ghosez, X. Gonze and J.-P. Michenaud, Europhys. Lett. **33**, 713 (1996).

[40] R. A. Cowley, Phys. Rev. 134, A981 (1964).

FIG. 1. Calculated phonon dispersion relations of $BaTiO_3$, $PbTiO_3$ and $PbZrO_3$ along various high-symmetry lines in the simple cubic Brillouin zone. A color has been assigned to each point based on the contribution of each kind of atom to the associated dynamical matrix eigenvector (red for the A atom, green for the B atom, and blue for the oxygens) [35]. Symmetry labels follow the convention of Ref. [40], with the A atom at the origin.

FIG. 2. Schematic three-dimensional view of the atoms labeled in Table III.

TABLE I. Lattice parameter (Å) at which DFPT calculations were performed, Born effective charges ($|e|$) and optical dielectric constant in the cubic perovskite structure for the three $ABO_3$ compounds.

| | $BaTiO_3$ | $PbTiO_3$ | $PbZrO_3$ |
|---|---|---|---|
| $a_{cell}$ | 4.00 | 3.97 | 4.12 |
| $Z^*_A$ | +2.74 | +3.87 | +3.93 |
| $Z^*_B$ | +7.32 | +7.04 | +5.89 |
| $Z^*_{O_\perp}$ | −2.14 | −2.57 | −2.50 |
| $Z^*_{O_\parallel}$ | −5.78 | −5.76 | −4.82 |
| $\epsilon_\infty$ | 6.75 | 8.24 | 6.97 |

TABLE II. Normalized dynamical matrix eigenvector for the unstable ferroelectric mode at Γ (z-polarization). The corresponding eigendisplacement in real space can be obtained by dividing each value by the appropriate mass factor $\sqrt{M_{ion}}$ .

| $ABO_3$ | A | B | $O_x$ | $O_y$ | $O_z$ |
|---|---|---|---|---|---|
| $BaTiO_3$ | +0.0178 | +0.6631 | −0.2842 | −0.2842 | −0.6311 |
| $PbTiO_3$ | +0.2314 | +0.4024 | −0.4792 | −0.4792 | −0.5704 |
| $PbZrO_3$ | +0.5033 | −0.1786 | −0.5738 | −0.5738 | −0.2374 |

TABLE III. Label assigned to various atoms in terms of their position in reduced coordinates.

| | | | | | |
|---|---|---|---|---|---|
| $A_0$ | ( 0.0, 0.0, 0.0) | $B_0$ | ( 0.5, 0.5, 0.5) | $O_1$ | ( 0.5, 0.5, 0.0) |
| $A_1$ | ( 0.0, 0.0, 1.0) | $B_1$ | ( 1.5, 0.5, 0.5) | $O_2$ | ( 0.5, 0.0, 0.5) |
| | | | | $O_3$ | (-0.5, 0.5, 0.0) |
| | | | | $O_4$ | ( 0.5, 0.5,-1.0) |
| | | | | $O_5$ | (-0.5, 0.0, 0.5) |

TABLE IV. Self-force constant (Ha/Bohr$^2$) on the different atoms in the unit cell.

| Atom | Direction | $BaTiO_3$ | $PbTiO_3$ | $PbZrO_3$ |
|---|---|---|---|---|
| $A_0$ | x=y=z | +0.0806 | +0.0247 | +0.0129 |
| $B_0$ | x=y=z | +0.1522 | +0.1393 | +0.2302 |
| $O_1$ | x=y | +0.0681 | +0.0451 | +0.0166 |
| | z | +0.1274 | +0.1518 | +0.2758 |

TABLE V. Selected longitudinal (‖), transverse (⊥) and cartesian ($\alpha\beta$) interatomic force constants (Ha/Bohr$^2$) between different pairs of atoms. The dipole-dipole (DD) and remaining short-range (SR) contribution, have been separated following the scheme described in Ref. [8].

| | | | $BaTiO_3$ | | | $PbTiO_3$ | | | $PbZrO_3$ | |
|---|---|---|---|---|---|---|---|---|---|---|
| Atom | | Total | DD | SR | Total | DD | SR | Total | DD | SR |
| $B_0$-$O_1$ | (‖) | +0.0094 | +0.2325 | −0.2231 | −0.0012 | +0.1865 | −0.1877 | −0.0687 | +0.1380 | −0.2067 |
| | (⊥) | −0.0211 | −0.0430 | +0.0218 | −0.0178 | −0.0417 | +0.0239 | −0.0100 | −0.0358 | +0.0258 |
| $B_0$-$B_1$ | (‖) | −0.0672 | −0.0368 | −0.0304 | −0.0615 | −0.0285 | −0.0330 | −0.0499 | −0.0211 | −0.0288 |
| | (⊥) | +0.0075 | +0.0184 | −0.0109 | +0.0065 | +0.0142 | −0.0077 | +0.0054 | +0.0105 | −0.0052 |
| $B_0$-$O_4$ | (‖) | +0.0156 | +0.0086 | +0.0070 | +0.0135 | +0.0069 | +0.0066 | +0.0106 | +0.0051 | +0.0055 |
| | (⊥) | +0.0009 | −0.0016 | +0.0007 | +0.0015 | −0.0015 | +0.0006 | +0.0012 | −0.0013 | +0.0002 |
| $B_0$-$A_0$ | (‖) | −0.0286 | −0.0212 | −0.0074 | −0.0277 | −0.0241 | −0.0036 | −0.0271 | −0.0216 | −0.0054 |
| | (⊥) | +0.0134 | +0.0106 | +0.0028 | +0.0157 | +0.0121 | +0.0036 | +0.0145 | +0.0108 | +0.0037 |
| | ($xx$) | −0.0006 | +0.0000 | −0.0006 | +0.0012 | +0.0000 | +0.0012 | +0.0007 | +0.0000 | +0.0007 |
| $A_0$-$O_1$ | (‖) | −0.0004 | +0.0114 | −0.0118 | +0.0108 | +0.0162 | −0.0054 | +0.0139 | +0.0169 | −0.0030 |
| | ($zz$) | −0.0108 | −0.0154 | +0.0045 | −0.0110 | −0.0181 | +0.0071 | −0.0103 | −0.0163 | +0.0060 |
| $A_0$-$A_1$ | (‖) | −0.0112 | −0.0052 | −0.0060 | −0.0108 | −0.0086 | −0.0022 | −0.0094 | −0.0093 | −0.0001 |
| | (⊥) | +0.0038 | +0.0025 | +0.0012 | +0.0054 | +0.0043 | +0.0011 | +0.0056 | +0.0047 | +0.0009 |

TABLE VI. Interatomic force constant matrix in cartesian coordinates (Ha/Bohr$^2$) between various pairs of oxygen atoms. Lines and columns of the matrix correspond respectively to x, y and z displacements for the first and second atom mentioned in the first column of the Table.

| Atoms | $BaTiO_3$ | $PbTiO_3$ | $PbZrO_3$ |
|---|---|---|---|
| $O_1$-$O_2$ | $\begin{pmatrix} +0.0037 & 0.0000 & 0.0000 \\ 0.0000 & -0.0087 & +0.0119 \\ 0.0000 & +0.0274 & -0.0087 \end{pmatrix}$ | $\begin{pmatrix} +0.0035 & 0.0000 & 0.0000 \\ 0.0000 & -0.0091 & +0.0123 \\ 0.0000 & +0.0271 & -0.0091 \end{pmatrix}$ | $\begin{pmatrix} +0.0038 & 0.0000 & 0.0000 \\ 0.0000 & -0.0065 & +0.0110 \\ 0.0000 & +0.0229 & -0.0065 \end{pmatrix}$ |
| $O_1$-$O_3$ | $\begin{pmatrix} -0.0019 & 0.0000 & 0.0000 \\ 0.0000 & +0.0017 & 0.0000 \\ 0.0000 & 0.0000 & +0.0091 \end{pmatrix}$ | $\begin{pmatrix} -0.0012 & 0.0000 & 0.0000 \\ 0.0000 & +0.0022 & 0.0000 \\ 0.0000 & 0.0000 & +0.0079 \end{pmatrix}$ | $\begin{pmatrix} -0.0012 & 0.0000 & 0.0000 \\ 0.0000 & +0.0021 & 0.0000 \\ 0.0000 & 0.0000 & +0.0055 \end{pmatrix}$ |
| $O_1$-$O_4$ | $\begin{pmatrix} -0.0003 & 0.0000 & 0.0000 \\ 0.0000 & -0.0003 & 0.0000 \\ 0.0000 & 0.0000 & -0.0321 \end{pmatrix}$ | $\begin{pmatrix} +0.0003 & 0.0000 & 0.0000 \\ 0.0000 & +0.0003 & 0.0000 \\ 0.0000 & 0.0000 & -0.0326 \end{pmatrix}$ | $\begin{pmatrix} -0.0010 & 0.0000 & 0.0000 \\ 0.0000 & -0.0010 & 0.0000 \\ 0.0000 & 0.0000 & -0.0362 \end{pmatrix}$ |
| $O_1$-$O_5$ | $\begin{pmatrix} -0.0006 & -0.0013 & +0.0007 \\ -0.0007 & +0.0013 & +0.0007 \\ +0.0013 & +0.0025 & +0.0013 \end{pmatrix}$ | $\begin{pmatrix} -0.0010 & -0.0013 & +0.0010 \\ -0.0010 & +0.0012 & +0.0011 \\ +0.0013 & +0.0022 & +0.0012 \end{pmatrix}$ | $\begin{pmatrix} -0.0010 & -0.0013 & +0.0010 \\ -0.0010 & +0.0011 & +0.0010 \\ +0.0013 & +0.0018 & +0.0011 \end{pmatrix}$ |

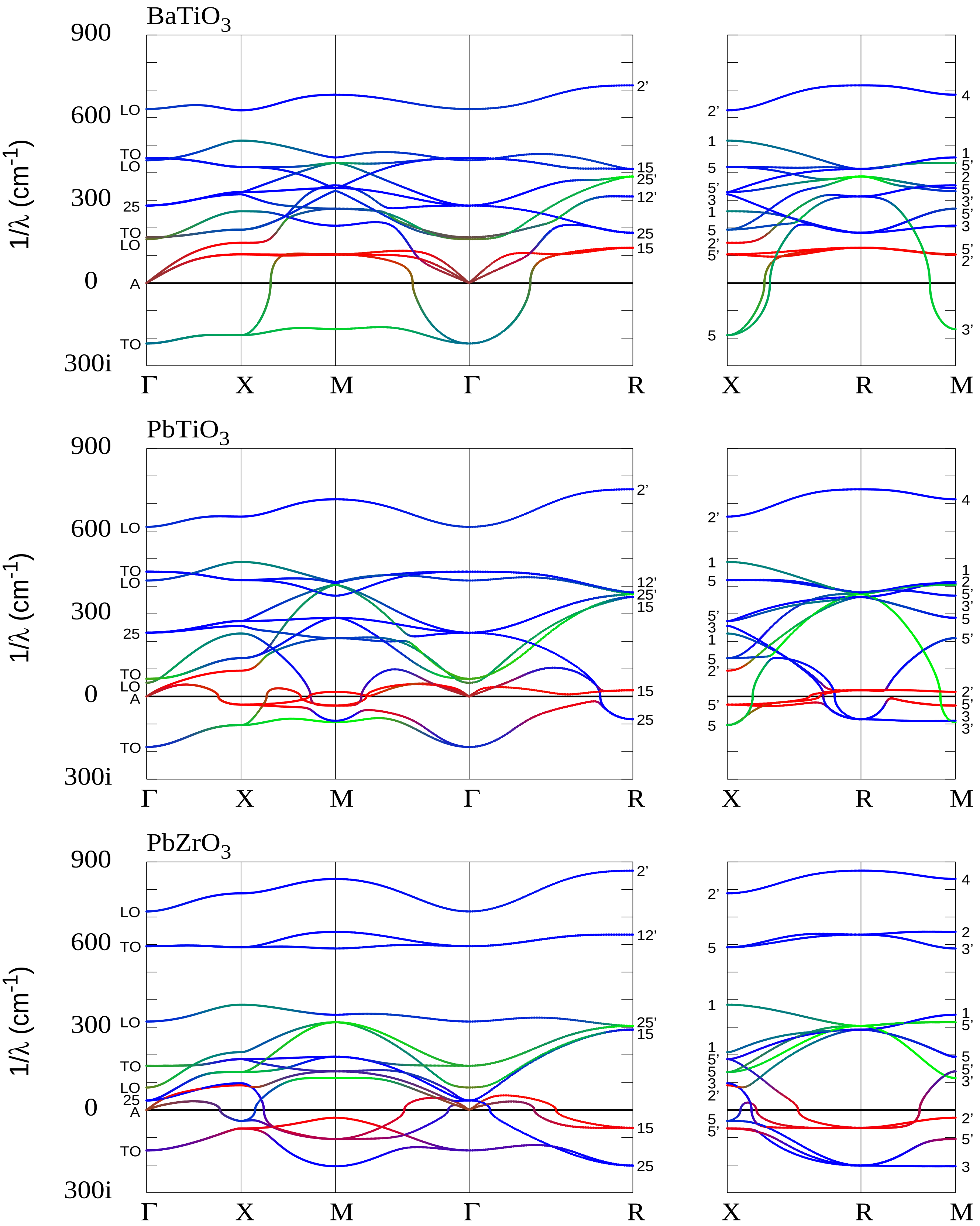
BaTiO$_3$
PbTiO$_3$
PbZrO$_3$
900
600
300
0
300i
1/λ (cm$^{-1}$)
LO
TO
25
A
2'
15
25'
12'
12'
1
2
3
3'
4
5
5'
Γ
X
M
Γ
R
X
R
M

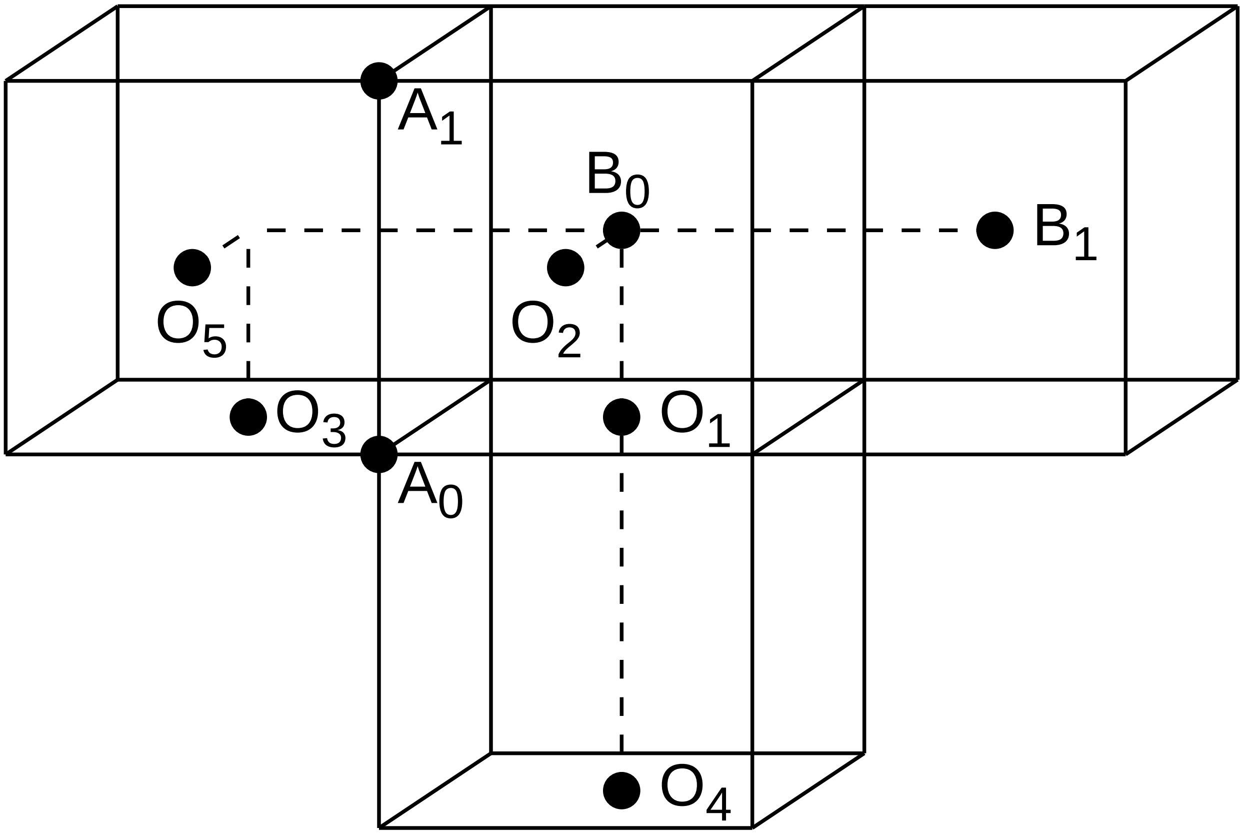
A$_1$
B$_0$
B$_1$
O$_5$
O$_2$
O$_3$
O$_1$
A$_0$
O$_4$